THE ASTROPHYSICAL JOURNAL, 278:564–574, 1984 March 15

MASSIVE STAR FORMATION IN NGC 6946

K. DEGIOIA-EASTWOOD AND G. L. GRASDALEN
University of Wyoming
AND
S. E. STROM AND K. M. STROM
Kitt Peak National Observatory[1]
Received 1982 July 8; accepted 1983 August 25

ABSTRACT

We present Hα measurements of the late-type spiral galaxy NGC 6946. Assuming an initial mass function, we use the Hα data to calculate the total star formation rate and efficiency of massive star formation as a function of galactocentric radius. We then attempt to determine the factors influencing these quantities by comparing them to the surface densities of H I and H_2 and the degree of compression suffered by the gas in spiral density wave theory. The rate of star formation is very closely correlated with the first power of the surface density of H_2, and somewhat less correlated with the degree of compression of the gas predicted by density wave theory. In contrast, the efficiency of massive star formation is roughly constant across the face of the galaxy. These results are consistent with results from previous studies of our own and other galaxies.

Subject headings: galaxies: individual — galaxies: stellar content — interstellar: matter — stars: formation

I. INTRODUCTION

The stimuli for star formation and the factors influencing star formation rates are topics not only interesting in themselves but closely tied to theories of galactic evolution and the propagation of spiral structure. In this paper we examine the rate and efficiency of massive star formation as a function of position in the late-type spiral galaxy NGC 6946 and try to determine the factors which influence these quantities.

Since tests of our understanding of current star formation in principle require observations of the newly formed stellar component and the associated hot ionized gas, as well as knowledge of the density and dynamics of the cool neutral and molecular gas, the well-studied ScI galaxy NGC 6946 represents an ideal laboratory for assessing the factors which affect these quantities. Extensive optical, infrared, H I, CO, and radio continuum measurements are already available. We have supplemented these data with measurements of the average Hα emission as a function of galactocentric radius. The number of observed Hα photons is directly proportional to the number of Lyman continuum photons present. Assuming a shape for the initial mass function (IMF) and calculating the expected number of Lyman continuum photons for an IMF of unit mass, we infer the mass of young stars present. We use these masses to calculate the star formation rate as a function of position. We also calculate the ratio of mass in young stars to the mass of hydrogen. This ratio is indicative of the efficiency of massive star formation.

Schmidt (1959) was the first to propose that the rate of star formation was dependent solely on the local density of interstellar gas and parameterized by a power law where the rate is proportional to some power of the density. Since then it has become clear that although time scales for star formation are likely to vary as the density to some negative power, they cannot depend on the density alone (Larson 1977).

Recently there have been many efforts to connect the global properties of spiral galaxies with the intrinsically local process of star formation. The most successful two of the attempts to explain the appearance of young objects in persistent spiral patterns and the continuum of physical properties along the Hubble sequence are those of spiral density wave theory (Roberts, Roberts, and Shu 1975) and stochastic self-propagating star formation (Seiden and Gerola 1979).

The prominent spiral structure and underlying red arms suggest that the spiral pattern in NGC 6946 may result from a spiral density wave rather than the process of stochastic self-propagating star formation. NGC 6946 is classified in Elmegreen's (1981) Near-Infrared Atlas of Spiral Galaxies as having a "grand design" or "global" spiral pattern instead of a "flocculent" pattern. Therefore we consider the galaxy well suited for comparison with density wave theory.

In this work we compare the behavior of the star formation rate and the efficiency of massive star formation with galactocentric radius to the surface densities of H I and H_2. We also compare the behavior of the star formation rate and the efficiency of massive star formation with galactocentric radius to that of the degree of compression suffered by the gas as predicted in density wave theory.

Our results show that the star formation rate is correlated with both the surface density of H_2 and the degree of compression suffered by the gas, but that the correlation with the surface density is the more significant of the two. We also find that the star formation rate is much more closely proportional to the first power of the surface density than to the second.

The efficiency of massive star formation is roughly constant across the face of the galaxy. It appears that the efficiency is intrinsically a local property and is not greatly influenced by

[1] Operated by the Association of Universities for Research in Astronomy Inc., under contract to the National Science Foundation.

global factors such as the interaction of the disk gas with a density wave.

In order to estimate the rate and efficiency of star formation, we decided to estimate the number of young stars through the presence of Lyman continuum photons. In an ionization-bounded nebula, the number of Lyman continuum photons is directly proportional to the number of photons emitted in a given Balmer line. We chose to observe Hα since it is not only the line which is brightest but also that which is least affected by extinction.

II. OBSERVATIONS

The optical data were taken from 1981 July through September on the Wyoming 2.3 m telescope with a photoelectric photometer equipped with a Varian S-surface photomultiplier tube. The circular variable filter used had bandwidths of 138 Å at Hα and 133 Å at λ6200, the wavelength chosen as the continuum.

The WIRO fast-mapping telescope control routines (Grasdalen *et al.* 1979; Hackwell, Grasdalen, and Gehrz 1982) were used to obtain digitized frames 120″ square. On the first observing run we imaged the inner regions of the galaxy using a format of 15 × 15 pixels with a 14″ diameter circular beam, sampling the area. The integration times per pixel were adjusted so that the total integration time for each individual frame, regardless of format, was about 10 minutes. The sky background, defined by areas found free of stars on the POSS, was monitored and subtracted for each frame. Each final frame used for simulated aperture photometry was the result of co-adding 5–10 individual frames, representing a total integration time for each final frame at each wavelength of 50–100 minutes. With seven final frames at each wavelength, covering about 28 arcmin^2, the total integration time is about 20 hours on the galaxy and about one-third of that time on blank sky.

We used the Wyoming image processing system to convert the raw data to a calibrated position-intensity matrix. The monochromatic air mass corrections were interpolated from the data of Hayes (1970) and taken to be 0.112 mag per air mass for Hα and 0.143 mag per air mass for λ6200. Sandage's (1973) model of the Galactic extinction was used in conjunction with a $1/\lambda$ reddening law to derive the values of the fluxes outside the galaxy. The data were reduced to absolute fluxes using observations of Stone's (1977) standard stars and the recalibration of Vega by Hayes and Latham (1975).

To check our photometry after these corrections we compared simulated aperture photometry of the nucleus at λ6200 with magnitudes extrapolated from the data of Ables (1971). Our magnitudes were within 3% of the calculated value for the 35″ aperture and within 8% of the value for the 51″ aperture.

In order to estimate the value of the underlying continuum at Hα from the flux at λ6200 it is necessary to choose a value for the continuum slope. Although the spectral energy distributions for the arm, interarm, and nuclear regions will all be slightly different, we decided to find an average value for the continuum slope and use it for all our data points. This results in a very slight overestimation of the Hα flux interarm (redder) regions and a very slight underestimation of the Hα flux in the arm and nuclear (bluer) regions. The *UBV* data of Ables for the nuclear region of NGC 6946 are not sufficient to estimate this average continuum slope. Schweizer (1976) has presented $V-R$ spot photometry of four ScI galaxies (de Vaucouleurs, de Vaucouleurs, and Corwin 1976, hereafter RC2). His apertures covered arm, interarm, and nuclear regions, and the average $V-R$ color was 0.70 mag with a standard deviation of only 0.08 mag for the four galaxies. This color corresponds

TABLE 1

UNCORRECTED FLUXES FOR 40″ SQUARE BOXES

Δα[a] (arcsec)	Δδ[b] (arcsec)	λ6200 Flux × 10^{12} (ergs cm^{-2} s^{-1})	λ6563 Flux × 10^{12} (ergs cm^{-2} s^{-1})
−47	−143	1.2	1.8
−47	−103	3.1	5.0
−47	−63	2.3	3.3
−47	−23	2.6	3.5
−47	17	1.9	2.9
−47	57	1.4	2.2
−47	97	0.83	1.6
−47	137	0.52	0.91
−7	−143	1.1	1.5
−7	−103	1.6	3.1
−7	−63	2.7	4.4
−7	−23	3.9	5.4
−7	17	4.3	7.2
−7	57	2.6	3.8
−7	97	1.6	2.9
−7	137	0.64	1.0
−7	177	0.64	1.1
33	−143	1.0	1.4
33	−23	2.5	3.6
33	17	2.8	4.2
33	57	2.2	3.1
33	97	2.0	4.3
33	137	0.99	1.4
33	177	0.60	0.88
73	−143	0.82	1.4
73	−103	0.89	1.5
73	−63	2.1	3.2
73	−23	1.8	3.1
73	17	2.0	3.3
73	57	2.2	3.6
73	97	1.5	2.7
73	137	0.76	1.4
73	177	0.50	0.76
113	−103	1.1	1.9
113	−63	1.1	1.9
113	−23	1.5	2.5
113	17	1.9	3.3
113	97	1.5	2.5
113	57	1.5	3.5
113	137	1.0	2.2
113	177	0.40	0.71
153	−143	0.64	1.2
153	−103	0.82	1.6
153	−63	0.94	1.5
153	−23	1.5	4.1
153	17	1.7	3.1
153	57	1.4	2.5
153	97	1.5	2.7
153	177	0.31	0.53
193	−23	0.85	1.3
193	17	0.97	1.4
193	57	1.2	2.0
233	57	1.4	4.0
273	57	0.44	1.0

[a] From nucleus, + to east, − to west.
[b] From nucleus, + to north, − to south.

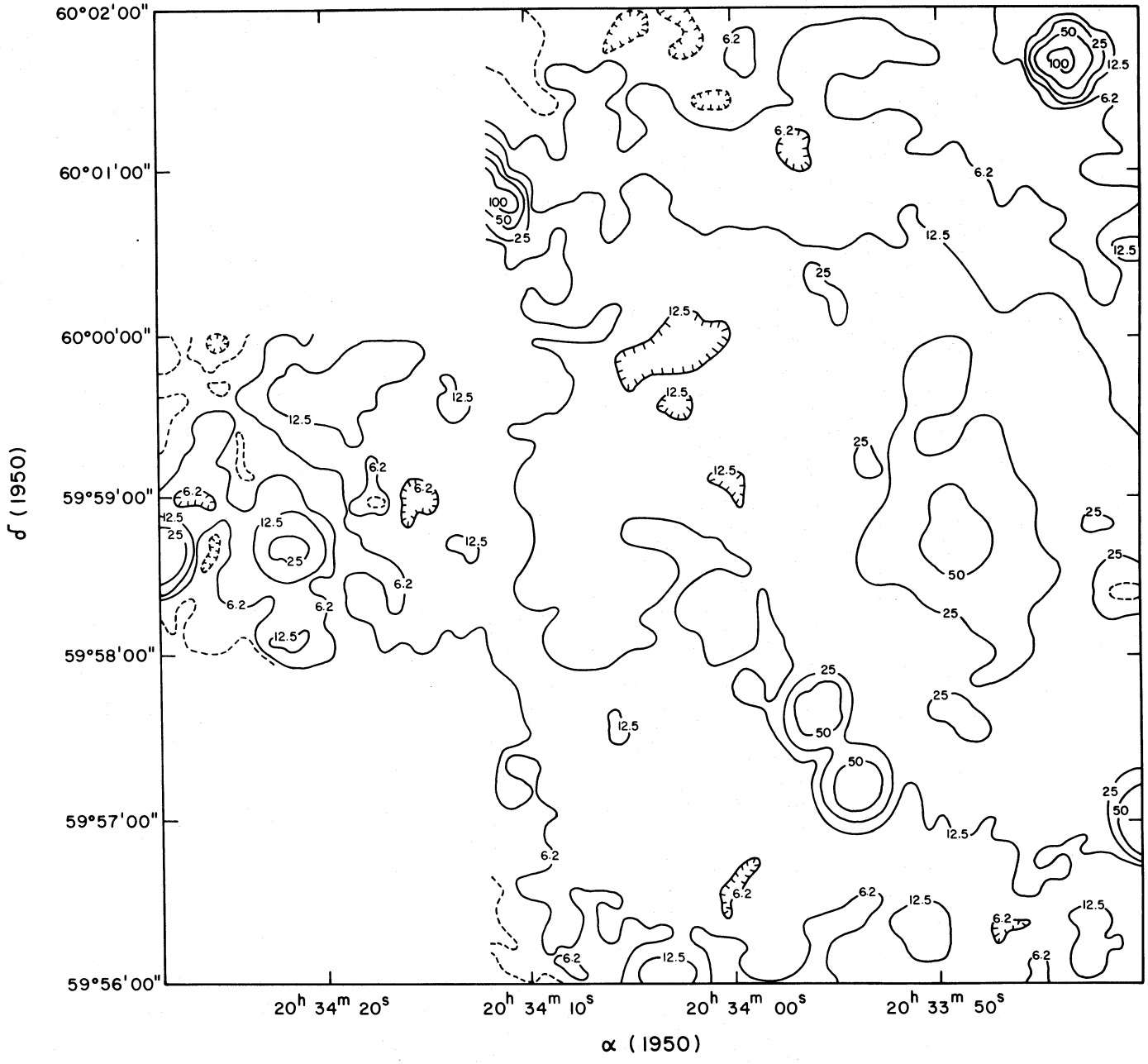

FIG. 1*a*

FIG. 1.—(*a*) A contoured representation of the continuum (λ6200) data. The dashed line is the lowest level, 3.12×10^{-16} ergs cm^{-2} s^{-1} arcsec^{-2}, in a 133 Å bandpass. Each remaining level is separated by a factor of 2 and labeled in units of 10^{-16} ergs cm^{-2} s^{-1} arcsec^{-2}. Galactic but not internal extinction corrections have been applied. (*b*) A gray scale representation of the data.

to that of a G8 III star. We used this slope between V and R to calculate the continuum slope between λ6200 and λ6563.

Data were obtained for seven final frames or 28 arcmin^2 in the visible disk ($D_{25} = 2.04$, RC2) of the galaxy, including the nucleus and the northeast "heavy" spiral arm which prompted Arp (1966) to place NGC 6946 in the Atlas of Peculiar Galaxies. The continuum and Hα emission data are reproduced in Figures 1 and 2. Since our intent was to compare the Hα to the H I and H_2 data, which were averaged as a function of galactocentric radius, we also averaged all our data as a function of radius using squares 40″ on a side. The signal-to-noise ratio of each square of this size is much higher than the signal to noise of each individual pixel. The calibrated, uncorrected flux values for each square are contained in Table 1. The squares were binned as a function of radius and the fluxes in each bin were then averaged. The radii were corrected for an inclination of 30° and a position angle of 62° (Rogstad and Shostak 1972). Our analyses are performed on the averaged data points at radii of 1′, 2′, 3′, and 4′ and simulated aperture photometry of the nucleus.

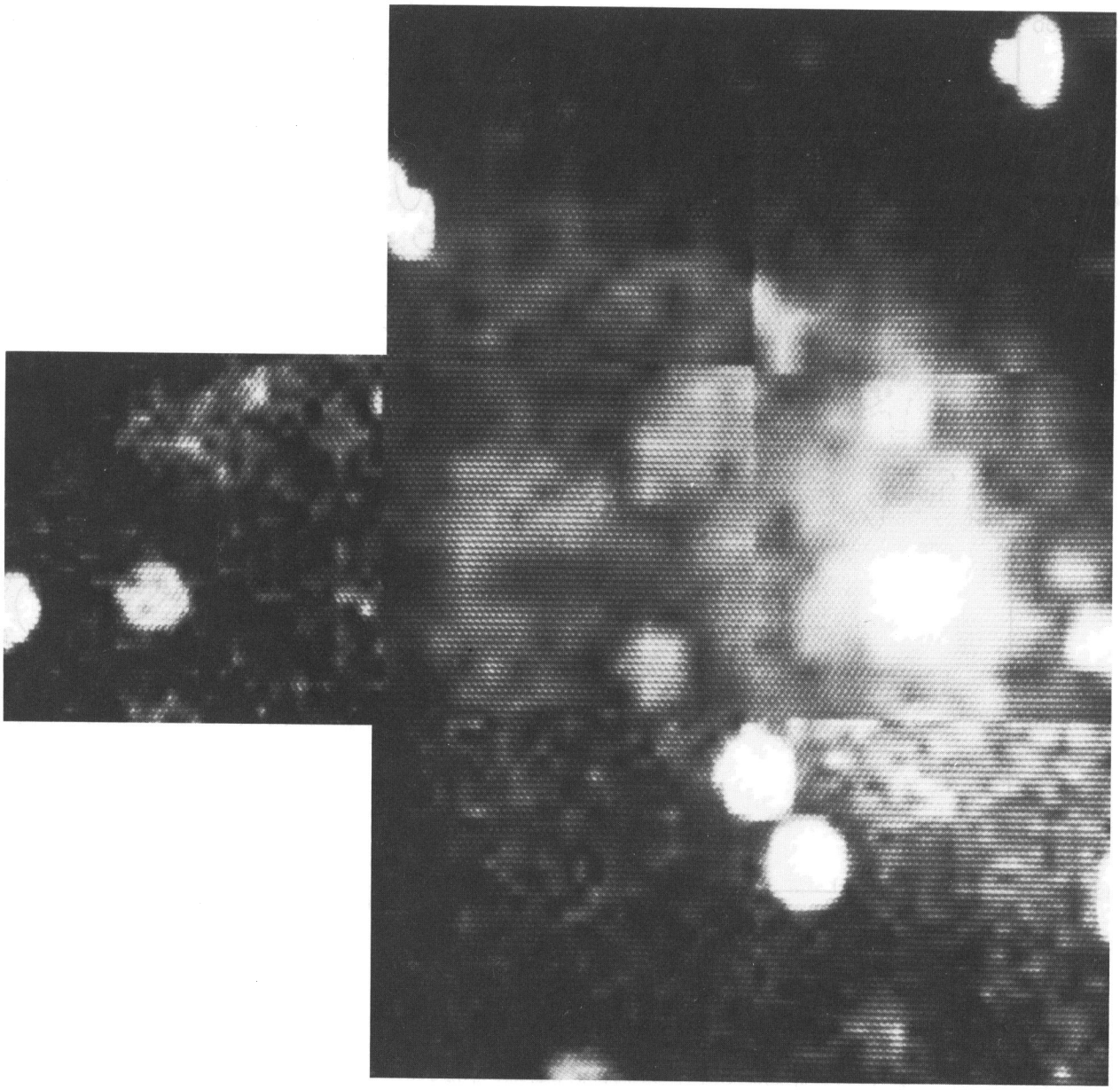

FIG. 1*b*

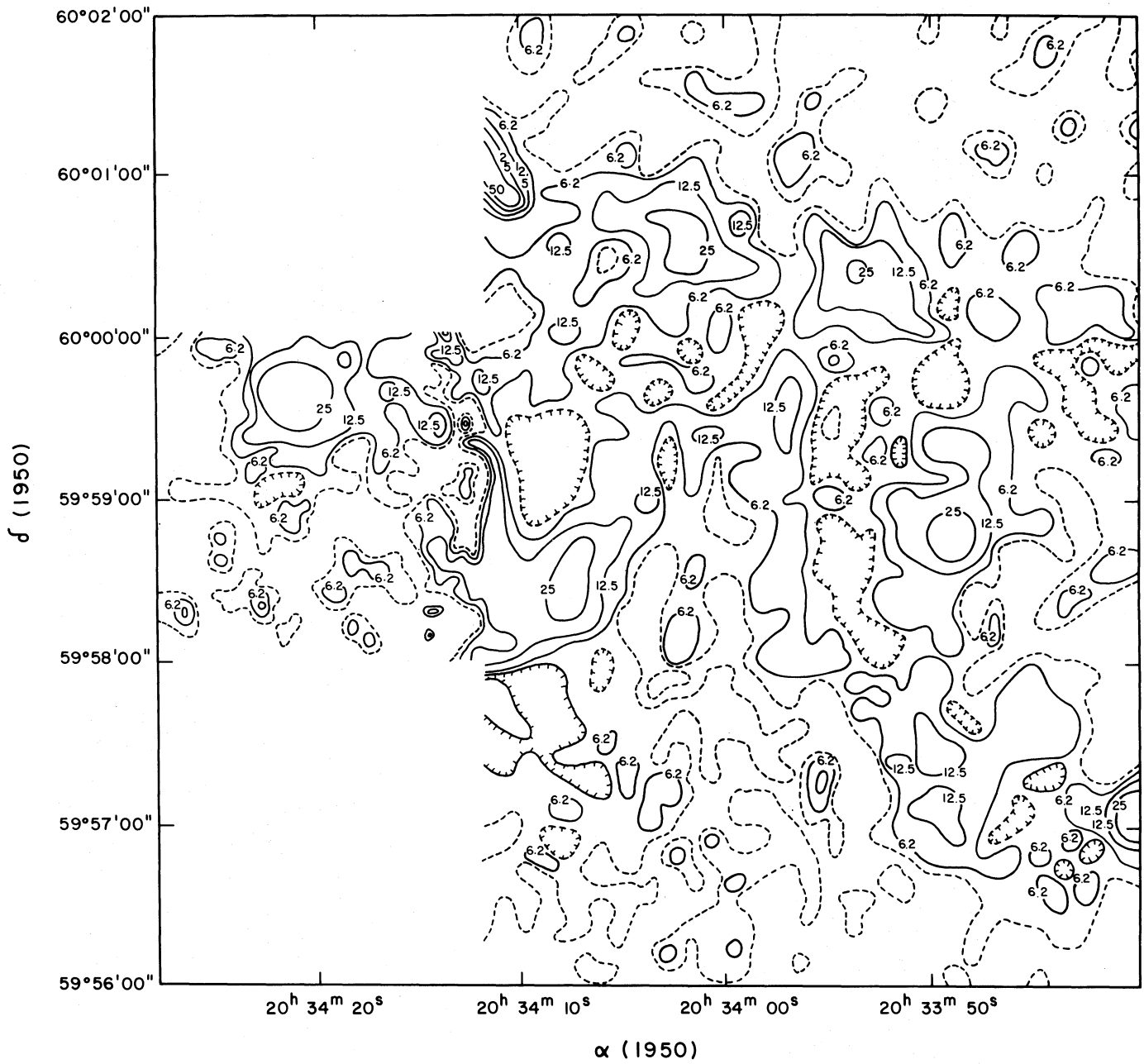

FIG. 2*a*

FIG. 2.—The same as Fig. 1 for the Hα emission only. Galactic extinction and continuum corrections but not [N II] or internal extinction corrections have been applied. Negative contours, such as those expected in the NW corner of the Hα field where the subtraction of a blue foreground star has left a "hole," are not plotted in the contoured representation. The two southern frames and the most eastern frame are of higher resolution than the others, and in order to show this no attempt has been made to smooth them in the gray scale representation. However, in the contoured representation the data have been sufficiently smoothed so that the contours are as simple as possible.

III. CORRECTIONS TO THE DATA

a) Corrections for [N II] *Emission within the Bandpass*

Since the [N II] lines at λλ6548 and 6583 are within our Hα bandpass, we corrected the emission for their presence. Smith (1975) found radial gradients in the observed reddening-corrected [N II]/Hα line intensity ratios for giant H II regions in late-type galaxies as a function of morphological type. We took the data for two late-type galaxies in his sample (M101 and M33, ScI and ScII–III, RC2) and performed a least squares fit on the relationship between [N II]/Hα and R/R_{25} (RC2). The result was $\log [\text{N II}]/\text{H}\alpha = -0.22-1.0(R/R_{25})$, which amounts to a contribution to the emission by the [N II] lines of 40% in the nucleus and 10% at 4′. Using this relationship we corrected our average values of the Hα emission as a function of radius.

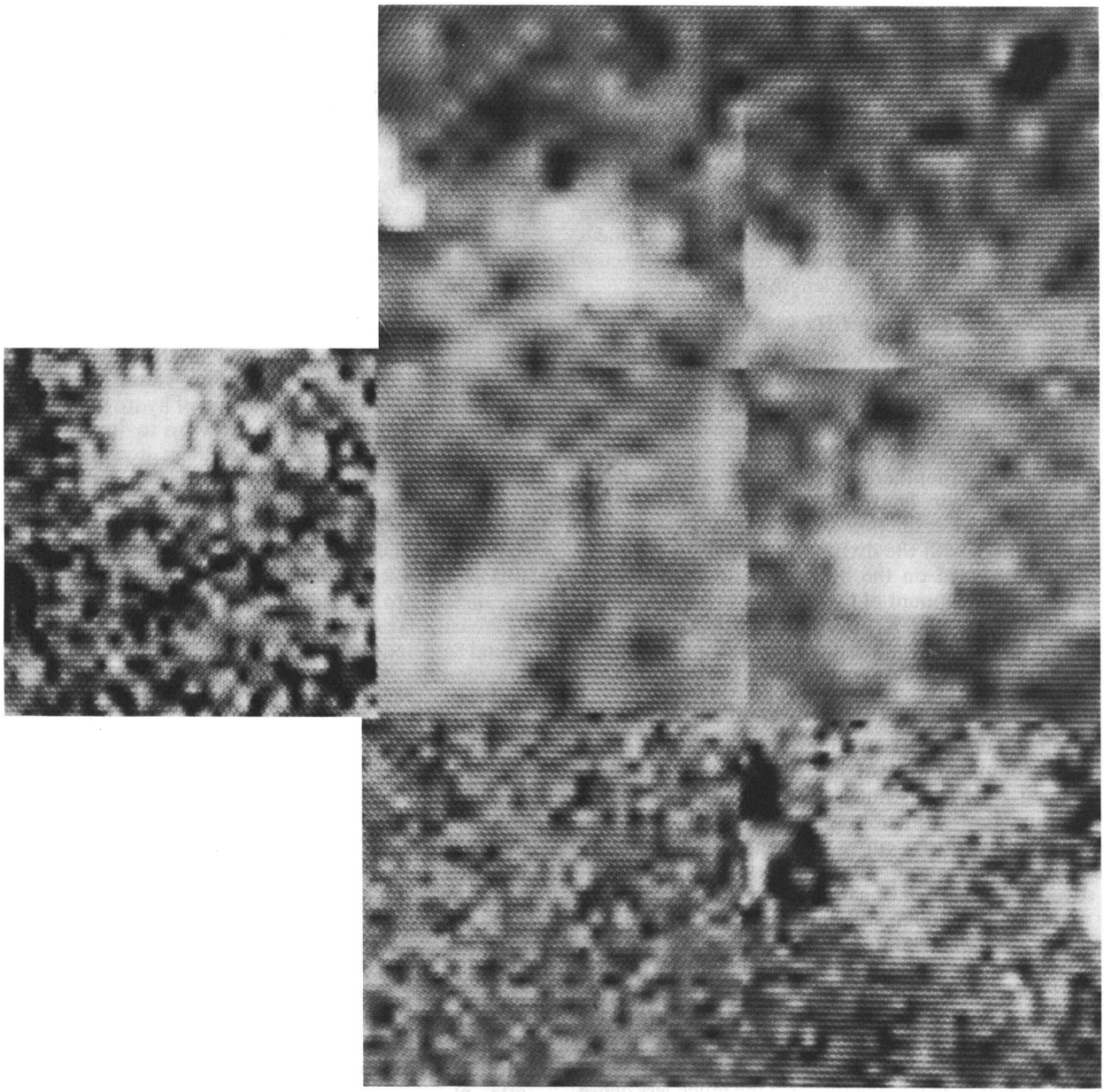

FIG. 2*b*

b) Estimation of Internal Extinction in the Disk

Since the basic purpose in measuring the Hα emission was to compare the mass of young stars inferred from its presence to the mass of hydrogen inferred from H I and CO radio emission, we needed to correct the visible data for internal extinction in the galaxy. We chose as the most realistic method that of combining one-half of the measured surface densities of H I (Rogstad and Shostak 1972) and H_2 inferred from CO (Young and Scoville 1981, using their conversion) with the empirical relationship between number of hydrogen atoms and color excess (Bohlin, Savage, and Drake 1978) to estimate the extinction to the central plane of the galaxy. The adopted values were $\langle N(\mathrm{H\ I} + \mathrm{H_2})/E(B-V)\rangle = 5.8 \times 10^{21}$ atoms $\mathrm{cm^{-2}}$ $\mathrm{mag^{-1}}$ and $R = A_v/E(B-V) = 3.1$. This method assumes that the dust-to-gas ratio and, implicitly, the heavy element abundances are the same in NGC 6946 as in our Galaxy. Using this method we find from 2.4 to 0.4 magnitudes of extinction at Hα in the disk where the extinction decreases roughly exponentially with a scale length of 1'.8.

c) Comparison of Corrected Hα with Radio Flux

When the extinctions derived from this method are applied to our Hα data, the corresponding thermal flux at 1415 MHz and 10.7 GHz can be calculated and compared to the data of van der Kruit, Allen, and Rots (1977) and Klein and Emerson (1981). There exists some uncertainty about the relative fractions of thermal and nonthermal flux at the shorter radio wavelengths. Using our final values of the Hα emission corrected for internal extinction we compared the corresponding radio fluxes with the division into thermal and nonthermal fluxes predicted on the basis of radio observations. Our estimates for the amount of thermal flux are smaller than those predicted by van der Kruit, Allen, and Rots (1977) by a factor of 1.5–2 and larger than the estimates of Klein and Emerson (1981) by about the same factor.

d) Estimation of Internal Extinction in the Nucleus

Comparing the calculated and measured radio fluxes we found that our computed value of the extinction for the nuclear region, 6.7 mag at Hα, was much too large. The radio flux calculated using this extinction was more than had been measured for the nucleus at either frequency.

This is evidence that a more realistic model than a condensed nucleus covered with a layer of gas and dust is necessary here. A more reasonable, although still naive, model is that of the optically thick case where stars, gas, and dust are uniformly mixed (cf. Rieke *et al.* 1980). In this case one sees in to only $1/\tau$. For the nucleus of NGC 6946, $1/\tau$ for $\tau = 6.7$ becomes the equivalent of only 2.1 mag of extinction. Adopting this value for the extinction brings the calculated radio emission into reasonable agreement with the measured values. We feel that the first, simpler model is adequate for the much less dense disk. The second method is more realistic in describing the nuclear region but still unreliable since it is unlikely that the dust and clumps of young objects are truly uniformly mixed. The actual Hα emission in the nuclear region should therefore be considered relatively uncertain. This model is consistent with the work of Lebofsky and Rieke (1979), who find that in the central 20″–30″ of NGC 6946 the silicate absorption feature at 9.8 μm implies an A_v greater than 50, while the optical colors indicate on the order of 1 mag of extinction.

IV. THE STAR FORMATION RATE IN THE DISK

a) Calculation of the SFR

In order to calculate the total star formation rate (SFR), several assumptions must be made. The first is that all Lyman continuum photons produced by young, hot stars spend themselves in ionizing hydrogen. Israel, Goss, and Allen (1975) found that giant H II complexes generally coincide in both dimension and position with neutral hydrogen maxima. One interpretation of this observation is that the H I is in front of and behind the H II, in which case they suggest that the H II complexes are generally ionization bound. The second assumption is that a given IMF holds everywhere in the galaxy, not only in the sense that the slope of the IMF remains constant but that high- and low-mass stars are formed simultaneously. The absolute value of the SFR depends on many other assumptions, but as long as these basic assumptions are satisfied then the relative values of the SFR as a function of position will be meaningful.

Following Smith, Biermann, and Mezger (1978) and Mezger (1978), we have computed the SFR by summing the number of Lyman continuum photons produced by a given IMF (Panagia 1973) and also summing the total mass along the IMF. Relating the number of photons to the flux of hydrogen emission using Osterbrock's (1974) method allows us to directly relate an Hα flux to the total main-sequence mass it represents. Dividing by the main sequence age of a 25 $M_\odot$ star, 6×10^6 years (Lamb, Iben, and Howard 1976), as representative of the life of an average H II region gives the total star formation rate in $M_\odot\ \mathrm{yr^{-1}}$. Dividing by the area producing the Hα emission makes the SFR per unit area, $M_\odot\ \mathrm{yr^{-1}}\ \mathrm{pc^{-2}}$, independent of the distance to the galaxy.

We calculated the SFR using two different IMFs: the traditional Salpeter (1955) power law and the three-segment power law representation of the more recent IMF derived by Miller and Scalo (1979). For each case we assumed that the lowest mass star formed had a mass of 0.1 $M_\odot$ and that no stars with a mass greater than 60 $M_\odot$ were formed. The Miller and Scalo IMF produces a SFR which is a factor of 6 greater than that produced by a Salpeter IMF from the same data. The relative values of the SFR as a function of position are not affected by the choice of IMF as long as the IMF is constant across the face of the galaxy. For purposes of comparison with other authors we will use the Salpeter IMF in the remainder of this paper.

The SFR is listed in Table 2 and is plotted as a function of radius in Figure 3. The error bars on the figure are indicative of the one standard deviation in the mean for the Hα emission. At each radius the sample of points consists of the set of 40″ square apertures corresponding to that radius. Because of the problems with modeling the extinction in the nucleus, no attempt has been made to estimate the errors inherent in the extinction correction. The value for the nucleus, obtained using synthetic aperture photometry, has been assigned error bars representing the photometric errors of less than 10%.

We next calculate the time necessary to deplete the present gas supply given the current SFR. The simplest form of this calculation ignores the return of gas to the interstellar medium by evolved stars and any infall of matter into the galaxy. This procedure results in the minimum time necessary for depletion. Performing this calculation with our data predicts an exhaus-

TABLE 2

CALCULATED AND OBSERVED PARAMETERS FOR NGC 6946

Radius (arcmin)	SFR[a] ($M_\odot$ Gyr^{-1} pc^{-2})	Efficiency[a] ($\times 10^4$)	$\sigma_{H\,I}$[b] (atoms cm^{-2})	σ_{H_2}[c] (atoms cm^{-2})	$(\Omega - \Omega_p)r$[d] (km s^{-1})
0	180	1.7	8×10^{20}	3×10^{22}	0
1	110	3.0	9×10^{20}	1×10^{22}	62
2	45	3.2	1×10^{21}	4×10^{21}	69
3	25	2.8	1×10^{21}	2×10^{21}	48
4	19	3.7	9×10^{20}	1×10^{21}	8.6

[a] Calculated using Salpeter IMF.
[b] Rogstad and Shostak 1972.
[c] Young and Scoville 1981.
[d] Calculated from H I rotation curve, assuming last H II region coincident with Ω_p.

tion time of 2.6 Gyr for the nucleus and 1.6 Gyr across the disk, equivalent to 13% and 8% of a Hubble time for $H_0 = 50$ km s^{-1} Mpc^{-1}. In a similar calculation Miller and Scalo (1979) find a range of consumption times of 1–3 Gyr for the solar neighborhood. They discuss galactic models consistent with these small times.

b) *Comparison of SFR with the Gas Density*

Given a SFR we can now compare its behavior as a function of galactocentric radius with the two theories mentioned in § I. The first is Schmidt's law, where it is proposed that

$$\mathrm{SFR} \propto \rho^n , \qquad (1)$$

where ρ is the gas volume density. In practice it is impossible to calculate the real volume density of gas in an external galaxy without knowing the scale height of the gas, and one looks for relationships of the type

$$\mathrm{SFR} \propto \sigma^k , \qquad (2)$$

where σ is the gas surface density. Many studies of this type have been carried out (cf. Madore 1977 and references therein), and generally k is found to have a value of between 1 and 2.

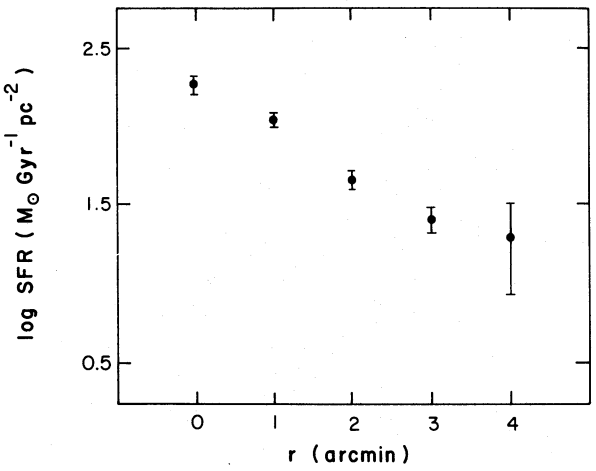

FIG. 3.—The log of the SFR plotted against galactocentric radius. The error bars are indicative of the one standard deviation of the mean for the set of corrected Hα fluxes in 40″ square boxes at each radius. Because of the difficulty with modeling the extinction in the nucleus no attempt has been made to estimate the errors inherent in the extinction correction. The value for the nucleus, obtained using synthetic aperture photometry, has been assigned its photometric errors of ±10%.

In our Galaxy the scale height of H I is fairly constant within the Sun's orbit and then increases gradually outside $R \approx 9.5$ kpc (Burton 1976). Our Galaxy is only slightly earlier in morphological type than NGC 6946. If the gas layer in NGC 6946 is also flat, then any value of j which we derive will be close to the desired value of n.

In Table 3 we present the results of a formal least squares analysis of log SFR versus log σ where σ is, respectively, the surface density of H I (Rogstad and Shostak 1972), H_2 inferred from CO (Young and Scoville 1981, using their conversion), and the sum of H I plus H_2. Included in the table are the power-law exponent k and linear correlation coefficient r. These results are strikingly similar to those of Talbot (1980) for our Galaxy and M83. Figure 4 shows the SFR compared to σ_{H_2} and $\sigma_{H\,I}$. The behavior of the SFR is closest to that of σ_{H_2}.

From Figure 5 it is clear that H_2 dominates over H I in the inner regions of NGC 6946. The surface densities become equal at roughly 4′, coincident with the spatial extent of our data. For this reason the correlations between the SFR and the surface densities of H_2 and the sum of H I plus H_2 are very similar. The SFR is undoubtedly correlated with σ_{H_2} and $\sigma_{H\,I+H_2}$, each having a correlation coefficient of 0.99. The relationship of SFR with $\sigma_{H\,I}$, however, has a correlation coefficient of −0.67, which does not easily lend itself to physical interpretation. Thus the SFR is seen to be highly correlated with σ_{H_2} but not correlated with $\sigma_{H\,I}$. This is not unexpected, however, since observations in the Milky Way show that massive stars tend to form in dense molecular clouds. Both these results are consistent with those of Talbot (1980) for our Galaxy and M83, who in both galaxies found the correlation highest for σ_{H_2} and obtained similarly negative coefficients for $\sigma_{H\,I}$.

The value of the exponent, k, is close to unity for both of our H_2-dominated correlations. Talbot found the exponent to be close to 1 for σ_{H_2} but closer to a value of 2 for the sum of H I plus H_2.

While considering his excellent correlation of H_2 (as inferred from CO) and the rate of star formation inferred from Hα,

TABLE 3

CORRELATIONS OF LOG SFR WITH OTHER PARAMETERS

Parameter	Slope k	Correlation Coefficient r
Log $\sigma_{H\,I}$	−6.69 ± 10.83	−0.67
Log σ_{H_2}	0.71 ± 0.04	0.99
Log $\sigma_{H\,I+H_2}$	0.85 ± 0.06	0.99
Log $(\Omega - \Omega_p)r$	0.54 ± 0.29	0.68

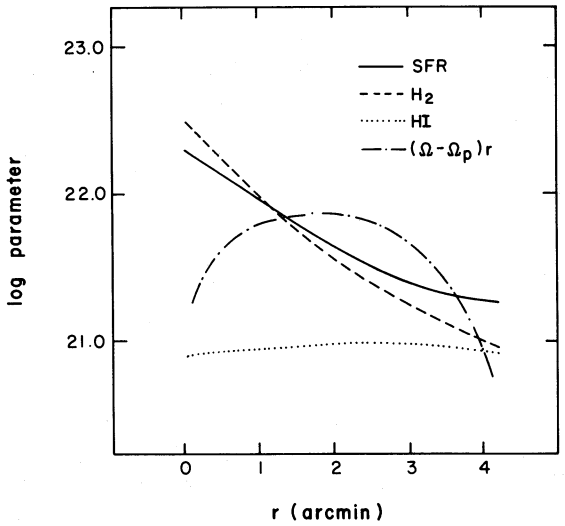

FIG. 4.—The SFR compared to other parameters. The solid line is log SFR + 20 in $M_\odot$ Gyr^{-1} pc^{-2}, the dashed line is σ_{H_2} in atom cm^{-2}, the dotted line is σ_{HI} in atom cm^{-2}, and the dot-dashed line is log $(\Omega - \Omega_p)r$ + 20 in km s^{-1}.

Talbot (1980) considers the possibility that the observed CO flux is excited by OB stars and that the correlation would then be trivial. This seems unlikely in view of observations of molecular clouds in our own Galaxy. The commonly observed $^{12}CO(J = 1–0)$ line is collisionally excited and, because of the molecule's high abundance, serves as one of the primary coolants for molecular clouds (Goldsmith and Langer 1978). When embedded in molecular clouds, OB stars heat the dust directly. In regions of high density ($n(H_2) > 10^5$ cm^{-3}) the dust and gas temperatures can couple through collisions, but these kinds of densities are generally found only in the hot cores of giant molecular clouds. Under typical conditions

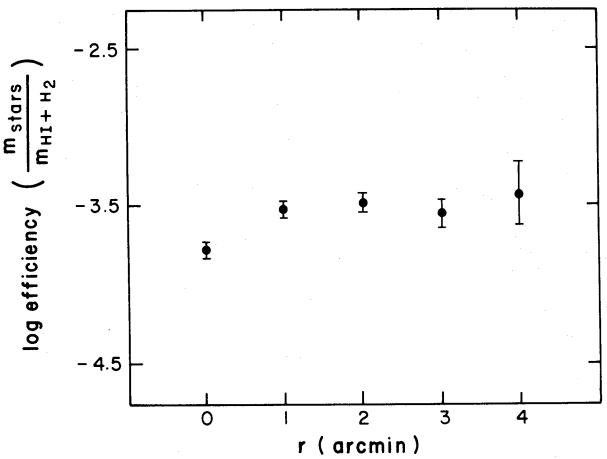

FIG. 5.—The efficiency of massive star formation, the ratio of the mass in hot stars to the mass in H I plus H_2, is shown as a function of galactocentric radius. The error bars are indicative of the one standard deviation of the mean for the set of corrected Hα fluxes in 40″ square boxes at each radius. Because of the difficulty with modeling the extinction in the nucleus, no attempt has been made to estimate the errors inherent in the extinction correction. The value for the nucleus, obtained using synthetic aperture photometry, has been assigned its photometric errors of ±10%.

there is imperfect coupling, and generally T_{gas} will be less than T_{dust}. Most of the CO luminosity in our Galaxy comes from the extended, cooler regions of the giant molecular clouds rather than their hot, dense cores or the smaller dark, cold molecular clouds.

An excellent example of a giant molecular cloud associated with an H II region is the Rosette molecular complex observed by Blitz and Thaddeus (1980). They find no detectable CO coincident with the Rosette nebula itself; apparently the molecules are largely destroyed by the ionizing and dissociating radiation. Furthermore, the strongest CO peak in the molecular complex shows no evidence of underlying star formation.

Even when dark clouds are directly associated with H II regions, analysis of the energetics suggests that only sometimes are the stars responsible for exciting the H II region also responsible for the heating of the dark cloud (see series by Evans *et al.* 1981 and references therein).

We feel that the correlation of H_2 and Hα simply represents the fact that massive stars are formed in molecular clouds. The very large beams in use for extragalactic CO observations suggest that with each measurement a sample of molecular clouds plus some associated H II regions are included in the beam. However, the OB stars do not directly excite the CO, so we are able to interpret the correlation in terms of the efficiency of massive star formation.

c) *Comparison with Gas Compression Predicted from Density Wave Theory*

We next wish to compare the observed SFRs with the dynamical quantity $(\Omega - \Omega_p)r$, which measures the compression of the gas behind a spiral shock. In spiral density wave theory, $(\Omega - \Omega_p)r \sin i$ is the velocity of the basic galactic rotation perpendicular to a spiral arm. For an idealized spiral pattern sin i, the pitch angle, is constant, and therefore $(\Omega - \Omega_p)r$ is an indication of the shock strength present (Roberts, Roberts, and Shu 1975; Strom 1980). In a simple model the square of this quantity should be proportional to the degree of compression suffered by the gas, and thus we expect the rate and efficiency of star formation to be related to this velocity in some way. We determined Ω_p, the pattern speed, by using the H I rotation curve to estimate the rotation velocity of the outermost H II region.

The correlation between the SFR and $(\Omega - \Omega_p)r$ is contained in Table 3. We find less of a correlation ($r = 0.68$) between the SFR and $(\Omega - \Omega_p)r$ than we do with σ_{H_2}; the SFR is proportional to $(\Omega - \Omega_p)r^{0.54\pm0.29}$.

It appears that the SFR is much more strongly influenced by the local gas density than by the shock strength predicted by spiral density wave theory.

V. CURRENT EPOCH EFFICIENCY OF GAS TO STAR CONVERSION IN THE DISK

A second interesting parameter which we calculated is that of the efficiency of massive star formation. Deriving the mass in newly formed stars in a 1600 $arcsec^2$ box as described in § IV and dividing that mass by the mass of H I plus H_2 produces a ratio which is representative of the efficiency. The value of the efficiency ranges from 1.7×10^{-4} to 3.2×10^{-4}. Armed with the assumption that stars are formed in dense molecular clouds, plus the results of the correlations of § IV,

we present only the efficiency of star formation with respect to the total gas density, H I plus H_2. Since H_2 is dominant, the results are very close to those obtained using just H_2.

The calculated values of the efficiency are included in Table 1, and Figure 5 is a plot of the log of the efficiency against radius. The error bars are indicative of the same scatter as described for Figure 3.

The efficiency is fairly constant to a radius of about 4′, or roughly 12 kpc, which is as far as our data is complete. In Figure 6 the efficiency is compared to three other quantities: the dynamical quantity $(\Omega - \Omega_p)r$, the surface density of H I plus H_2, and the square of that surface density. Although the formal correlations between the efficiency and $(\Omega - \Omega_p)r$ and the surface density are not included, they all show the exponent to be not much different from zero, which confirms the visual impression that the efficiency is roughly constant.

The value of $(\Omega - \Omega_p)r$, calculated from the H I rotation curve, reaches a maximum around a radius of 2′ and then drops to zero just outside 4′. The behavior of the efficiency is actually roughly similar to $(\Omega - \Omega_p)r$ in the inner part of the galaxy but shows no signs of dropping off, although the scatter in the last point is very large.

In NGC 6946, then, the efficiency of massive star formation seems independent of global dynamical properties and may depend only on the conditions present at the actual sites of star formation.

VI. THE EFFICIENCY OF STAR FORMATION IN THE NUCLEUS

From our previous discussion it is clear that the determination of Hα in the nucleus is not adequate to estimate the number of UV photons and the current star formation. There are two other methods available: to use radio continuum or far-infrared thermal fluxes to infer the number of UV photons.

Van der Kruit, Allen, and Rots (1977) find the nucleus to be less than 3″ in diameter. Their nuclear flux densities for 6.0 cm and 21.2 cm correspond to 1.1×10^4 O5 stars and 2.8×10^4 O5 stars, respectively, assuming that all the flux is thermal and knowing the flux of Lyman continuum photons from an O5 star (Panagia 1973). These are consistent since emission at 21.2 cm is not expected to be entirely thermal. Klein and Emerson (1981) give a value of 44 mJy for the nuclear flux density at 2.8 cm, which corresponds to 1.7×10^4 O5 stars.

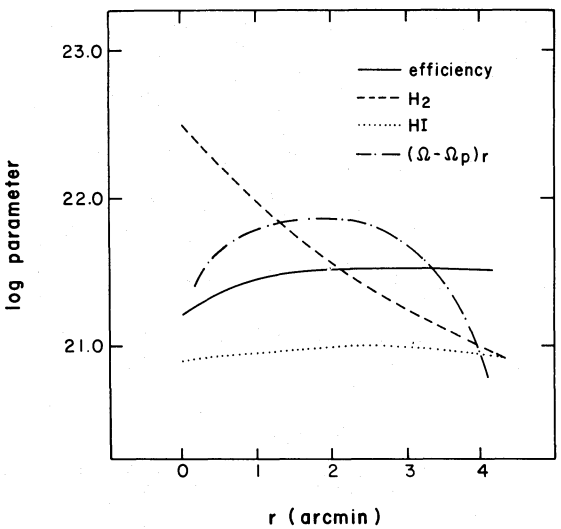

FIG. 6.—The efficiency of massive star formation compared with other parameters. The solid line is log $m_{stars}/(m_{H\,I+H_2})$ + 25, the dashed line is σ_{H_2} in atoms cm^{-2}, the dotted line is $\sigma_{H\,I}$ in atom cm^{-2}, and the dot-dashed line is log $(\Omega - \Omega_p)r$ + 20 in km s^{-1}.

Infrared measurements at 10 and 20 μm in a 5″ beam (Rieke and Lebofsky 1978) indicate that the infrared radiation is thermal emission from dust at a temperature of about 200 K. The later discovery of a silicate absorption feature (Lebofsky and Rieke 1979) confirms the presence of dust. The total luminosity of the blackbody curve which best fits the data is that which would be produced by 1.6×10^4 O5 stars hidden by the dust and having all their energy reradiated by the dust in the infrared. These data indicate that there is active star formation in the nucleus and that little optical emission is expected since it is all hidden.

A lower limit to the efficiency of massive star formation in the nucleus can be calculated by dividing the mass of 1.5×10^4 O5 stars by the mass of H I plus H_2 present in a 5″ beam. Unfortunately the value is only a lower limit because the half-power beam width used in the CO study (Young and Scoville 1981) was 50″, and thus the nuclear value for the H_2 surface density represents an average over that area. The value within a true 5″ beam would undoubtedly be higher. Calculated in this manner, the lower limit to the efficiency is 7.1×10^{-4}. When plotted on Figure 3, this value falls within the error bars of the efficiency for a 1600 arcsec^2 box centered on the nucleus.

VII. GENERALITY OF RESULTS

As discussed in § IV, the high correlation of the SFR with σ_{H_2} reproduces Talbot's (1980) results for the Milky Way Galaxy and M83, as well as the absence of a correlation between the SFR and $\sigma_{H\,I}$. The range and absolute values of the SFR for M83 quoted by Jensen, Talbot, and Dufour (1981, hereafter JTD) can be compared with ours by noting that in the notes to their Table 1, JTD give a conversion factor of 8.58×10^{60} Lyman continuum photons per solar mass for their IMF. With our slightly different assumptions we get an equivalent number of 5.09×10^{60}. This gives us SFR values about 70% higher than those of JTD for the same Hα flux. Their values for different positions in M83 range from 5 to 101 $M_\odot$ pc^{-2} Gyr^{-1}; our values for NGC 6946 range from 8 to 180 $M_\odot$ pc^{-2} Gyr^{-1}. Given the difference in conversion factors, our values for the SFR cover the same range as those of JTD.

Smith, Biermann, and Mezger (1978) and Mezger (1978) report a range of values for the SFR in our Galaxy of about 0.005 to 400 $M_\odot$ Gyr^{-1} pc^{-2}. They use radio continuum flux as a measure of the number of Lyman continuum photons. Their conversion factor, which produces a SFR a factor of 15 higher than ours, uses their estimate of the average age of a radio H II region, 5×10^5 yr. Mezger (1978) later revised his values of the SFR downward by about 30%. Thus the equivalently derived SFR in our Galaxy is lower by a factor of 10–15 than that in NGC 6946.

Although Hunter, Gallagher, and Rautenkranz (1982) do not specify their conversion factor, they use a Miller and Scalo IMF instead of a Salpeter IMF as well as a slightly different method of calculation to obtain the SFR from optical hydrogen lines. Their values for the SFR in the central regions of a sample of irregular galaxies range from 2 to 1000 $M_\odot$ pc^{-2} Gyr^{-1}. If we had used the Miller and Scalo IMF our values

would have been a factor of 6 higher, giving us a range of roughly 50 to 1000. Despite the uncertainties in assuming a shape for the IMF, the values of our SFR seem to be within the ranges measured by others in external galaxies.

If the gas layer in NGC 6946 is flat, then our results show that the SFR is much more closely related to the first power of the gas density than to the second. This is consistent with the recent model of Vader and deJong (1981), who constructed a model of kinematical and chemical evolution in the solar neighborhood, explicitly treating the variation in z of all quantities as well as the process of stellar acceleration. They found that models with $n = 1$ rather than $n = 2$ best explained the observed paucity of metal-poor stars.

Although the range of values measured for the SFR is consistent with those in other galaxies, and the correlations of the SFR with gas surface density are very similar to those found by Talbot (1980) for our Galaxy and for M83 (see § IV), the behavior of the SFR and efficiency with radius are dissimilar to those found by Talbot (1980) and JTD for our Galaxy and for M83. Instead of a monotonically decreasing SFR, they find the SFR to peak at about 4 kpc for our Galaxy and at about 2 kpc for M83. Talbot's quantity ν_h, the SFR per unit area, is equivalent to our efficiency. He finds that in both those galaxies ν_h is very sharply peaked at about the same radii where the SFR peaks.

We note here that Young and Scoville (1982) also found the CO distribution in NGC 6946 to be markedly different than in our Galaxy. NGC 6946 exhibits a smooth decrease of CO intensity with radius, whereas our Galaxy has a central peak, a "hole" from 1 to 4 kpc, and a molecular cloud ring at about 5 kpc. The CO distribution in M83 is similar to that in our Galaxy. It seems therefore that the behavior of the SFR is directly related to the distribution of CO in all three galaxies.

In summary, then, the major results of this work are:

1. In NGC 6946 the rate of star formation as derived from hydrogen emission is a decreasing function of galactocentric radius and is very closely correlated with the first power of the surface density of H_2 and somewhat less correlated with the dynamical quantity $(\Omega - \Omega_p)r$.
2. The efficiency of massive star formation (derived from the ratio of Hα emission to CO emission) is roughly constant as a function of galactocentric radius.
3. The values for the star formation rate are consistent with those found for other galaxies, but the behavior of the star formation rate and efficiency with radius are different than those found in our Galaxy and in M83.

We thank the referee, Eric Jensen, for many constructive comments. This work was supported by the National Science Foundation.

REFERENCES

Ables, H. D. 1971, *Pub. US Naval Obs., Ser. 2*, Vol. **20**, Part 4.
Arp, H. C. 1966, *Ap. J. Suppl.*, **14**, 1.
Blitz, L., and Thaddeus, P. 1980, *Ap. J.*, **241**, 676.
Bohlin, R. C., Savage, B. D., and Drake, J. F. 1978, *Ap. J.*, **224**, 132.
Burton, W. B. 1976, *Ann. Rev. Astr. Ap.*, **14**, 275.
de Vaucouleurs, G., de Vaucouleurs, A., and Corwin, H. C. 1976, *Second Reference Catalogue of Bright Galaxies*, (Austin: University of Texas Press) (RC2).
Elmegreen, D. M. 1981, *Ap. J. Suppl.*, **47**, 229.
Evans, N. J., Blair, G. N., Harvey, P., Israel, F., Peters, W. L., Scholtes, M., deGraauw, T., and Vanden Bout, P. 1981, *Ap. J.*, **250**, 200.
Goldsmith, P. F., and Langer, W. D. 1978, *Ap. J.*, **222**, 881.
Grasdalen, G. L., Herzog, A. D., Hackwell, J. A., and Gehrz, R. D. 1979, *Bull. AAS*, **11**, 712.
Hackwell, J. A., Grasdalen, G. L., and Gehrz, R. D. 1982, *Ap. J.*, **252**, 250.
Hayes, D. S. 1970, *Ap. J.*, **159**, 165.
Hayes, D. S., and Latham, D. W. 1975, *Ap. J.*, **197**, 593.
Hunter, D. A., Gallagher, J. S., and Rautenkranz, D. 1982, *Ap. J. Suppl.*, **49**, 53.
Israel, F. P., Goss, W. M., and Allen, R. J. 1975, *Astr. Ap.*, **40**, 421.
Jensen, E. B., Talbot, R. J., and Dufour, R. J. 1981, *Ap. J.*, **243**, 716 (JTD).
Klein, U., and Emerson, D. T. 1981, *Astr. Ap.*, **94**, 29.
Lamb, S. A., Iben, I., and Howard, W. M. 1976, *Ap. J.*, **207**, 209.
Larson, R. B. 1977, in *The Evolution of Galaxies and Stellar Populations*, ed. B. M. Tinsley and R. B. Larson (New Haven: Yale University Observatory), p. 97.
Lebofsky, M. J., and Rieke, G. H. 1979, *Ap. J.*, **229**, 111.
Madore, B. F. 1977, *M.N.R.A.S.*, **178**, 1.
Mezger, P. G. 1978, *Astr. Ap.*, **70**, 565.
Miller, G. E., and Scalo, J. M. 1979, *Ap. J. Suppl.*, **41**, 513.
Osterbrock, D. E. 1974, *Astrophysics of Gaseous Nebulae* (San Francisco: W. H. Freeman), p. 121.
Panagia, N. 1973, *A.J.*, **78**, 929.
Rieke, G. H., and Lebofsky, M. J. 1978, *Ap. J. (Letters)*, **220**, L37.
Rieke, G. H., Lebofsky, M. J., Thompson, R. I., Low, F. J., and Tokunaga, A. T. 1980, *Ap. J.*, **238**, 24.
Roberts, W. W. Roberts, M. S., and Shu, F. H. 1975, *Ap. J.*, **196**, 381.
Rogstad, D. H., and Shostak, G. S. 1972, *Ap. J.*, **176**, 315.
Salpeter, E. E. 1955, *Ap. J.*, **121**, 161.
Sandage, A. 1973, *Ap. J.*, **183**, 711.
Schmidt, M. 1959, *Ap. J.*, **129**, 243.
Schweizer, F. 1976, *Ap. J. Suppl.*, **31**, 313.
Seiden, P. E., and Gerola, H. 1979, *Ap. J.*, **233**, 56.
Smith, H. E. 1975, *Ap. J.*, **199**, 591.
Smith, L. F., Biermann, P., and Mezger, P. G. 1978, *Astr. Ap.*, **66**, 65.
Stone, R. P. S. 1977, *Ap. J.*, **218**, 767.
Strom, S. E. 1980, *Ap. J.*, **237**, 686.
Talbot, R. J. 1980, *Ap. J.*, **235**, 821.
Vader, J. P., and deJong, T. 1981, *Astr. Ap.*, **100**, 124.
van der Kruit, P. C., Allen, R. J., and Rots, A. H. 1977, *Astr. Ap.*, **55**, 421.
Young, J., and Scoville, N. 1982, *Ap. J.*, **258**, 467.

K. DEGIOIA-EASTWOOD: Washburn Observatory, University of Wisconsin, 475 North Charter Street, Madison, WI 53706

G. L. GRASDALEN: Department of Physics and Astronomy, University of Wyoming, Box 3905 University Station, Laramie, WY 82071

K. M. STROM and S. E. STROM: Department of Physics and Astronomy, University of Massachusetts, Graduate Research Center, Amherst, MA 01003